Note: The sentence being partly modified is in red, and that being newly added are in blue. The contents in black are not changed.

Rhenium-osmium abundance and isotopic compositions of massive sulfides from modern deep-sea hydrothermal systems: Implications for vent associated ore forming processes

Zhigang Zeng[a,*], Shuai Chen[a], David Selby[b], Xuebo Yin[a], Xiaoyuan Wang[a]

[a] Seafloor Hydrothermal Activity Laboratory of the Key Laboratory of Marine Geology and Environment, Institute of Oceanology, Chinese Academy of Sciences, Qingdao 266071, China

[b] Department of Earth Sciences, University of Durham, Durham DH1 3LE, UK

*Corresponding author. Email address: zgzeng@ms.qdio.ac.cn (Z.-G. Zeng). Postal address: Seafloor Hydrothermal Activity Laboratory of the Key Laboratory of Marine Geology and Environment, Institute of Oceanology, Chinese Academy of Sciences, 7 Nanhai Road, Qingdao 266071, China.

Tel.: +86 532 82898525; fax: +86 532 82898525.

ABSTRACT

Studies of rhenium (Re) and osmium (Os) concentrations and isotopic compositions in seafloor hydrothermal sulfides are an important tool for understanding the evolution of hydrothermal systems, allowing the determination of both metal sources and reconstructing the physicochemical conditions of their deposition. The Re-Os concentrations and isotopic compositions of 38 massive sulfide samples have been studied in different hydrothermal fields from the East Pacific Rise (EPR), Mid-Atlantic Ridge (MAR), Central Indian Ridge (CIR), Southwest Indian Ridge (SWIR), and Back-Arc Basin (BAB). The majority of the sulfides possess $^{187}Os/^{188}Os$ that span a narrow range (1.004 to 1.209), which is most easily explained as a seawater-derived component. This may suggest that those initial $^{187}Os/^{188}Os$ isotope compositions of ancient seafloor hydrothermal sulfide deposits which were formed by the mixing process between seawater and hydrothermal fluid, are possible for analysing ancient seawater Os components. Only two of samples (MAR05-TVG1-10-2 and MAR05-TVG1-21 from the Logatchev hydrothermal field (LHF), MAR) possess moderately less radiogenic $^{187}Os/^{188}Os$ (0.645 to 0.730), which may reflect the less extent of hydrothermal fluid-seawater mixing during hydrothermal ore-forming process.

The rhenium and Os concentrations and $^{187}Re/^{188}Os$ ratios of pyrite and Fe-Cu sulfide mineral aggregates (avg Re 11.46 ppb; avg Os 17.76 ppt; avg $^{187}Re/^{188}Os$ 11,980.4; *n* = 24) are usually higher than that of sphalerite or Zn-enriched sulfide mineral aggregate samples (avg Re 0.31 ppb; avg Os 7.09 ppt; avg $^{187}Re/^{188}Os$ 206.99; *n* = 9),

suggest that Re and Os are more likely to be incorporated into Fe- and Fe-Cu sulfide mineral facies. A significant positive correlation is observed between Os/Re ratios and Pb concentrations in the sulfide samples from the Edmond hydrothermal field (EHF), whereas Pb-enriched of sulfide is characteristic of low-temperature paragenetic association, suggesting that Os enriched under low-temperature (< 200°C) condition. In addition, our Re-Os data are used to estimate that modern seafloor sulfide deposits contain roughly 0.6 to 44 tonnes (avg 4 tonnes, n = 38) of Re, and 1 to 48 kg (avg 8 kg, n = 38) of Os. The Os flux of global low-temperature hydrothermal fluids to vents is about 11 kg per year, and the excess Os (i.e. Os not incorporated in sulfides) may be carried and become bound in metalliferous sediment, Fe-Mn crusts and nodules distal to the hydrothermal vents.

Keywords: Re-Os isotopes; massive sulfides; seafloor hydrothermal systems

1. Introduction

The study of ore-forming processes of metals is a key to understand the formation, distribution, type, and size of seafloor sulfide deposits (e.g. Baker and German, 2004; Fouquet, 1997; Hannington et al., 2005, 2011; Rona, 2003). The strongly siderophile and chalcophile (i.e. easily dissolved in iron-rich and/or sulfur-rich liquids) (Shirey and Walker, 1998) nature of both Re and Os means these elements are often incorporated directly into sulfide phases. As a result Re-Os isotopic compositions of seafloor massive sulfides provide information about the sources of metal and ore-forming conditions (e.g. Brügmann et al., 1998; Morelli et al., 2004; Ravizza et al., 1996). To date, the Re and Os distribution and isotope composition in massive sulfides has been determined for some ancient volcanic-hosted massive sulfide (VHMS) deposits in the Iberian Pyrite Belt (Mathur et al., 1999; Munhá, 2005), Southern Urals (Gannoun et al., 2003; Tessalina et al., 2008), Sanbagawa metamorphic belt (Nozaki et al., 2010, 2013), Red Dog deposit of the Brooks Range belt (Morelli et al., 2004), Kuroko ore deposits of the Hokuroku District (Terakado, 2001a), Wanibuchi Mine (Terakado, 2001b), Gacun deposit of southwestern China (Hou et al., 2003), and modern Trans-Atlantic Geotraverse (TAG) hydrothermal field on the MAR (Brügmann et al., 1998; Ravizza et al., 1996). In the Iberian Pyrite Belt, calculated initial $^{187}Os/^{188}Os$ values are ~0.37, which suggest that the continental margin sediments or the volcanic rocks are plausible sources for ore-forming metals (Mathur et al., 1999). In the Southern Urals, Russia, Re concentrations are quite homogenous throughout the hydrothermal system (10 to 30 ppb); however the Os

89 concentrations increase upwards in the hydrothermal system (98 to 1,000 ppt), which
90 colud be explained by progressive leaching of Os by high-temperature fluid and its
91 re-deposition (Tessalina et al., 2008). Further, the Os isotopic compositions in Urals
92 ore facies (including massive sulfide) is controlled by the mixture of hydrothermal
93 fluid and seawater (Tessalina et al., 2008), with the majority of Os in the massive
94 sulfides being derived from the submarine high-level mantle rocks (Gannoun et al.,
95 2003). The Sanbagawa metamorphic belt of southwest Japan, hosts numerous
96 Kimmeridgian Iimori Besshi-type deposits for which sulfide minerals possess a wide
97 range of $^{187}Os/^{188}Os$ values (~ 0.10 to 0.67; Nozaki et al., 2013). The more radiogenic
98 initial $^{187}Os/^{188}Os$ values for sulfides from the Iimori Besshi-type are suggested to be
99 caused by the entrainment of contemporaneous seawater with a more radiogenic
100 $^{187}Os/^{188}Os$ value into the pristine hydrothermal fluid (Nozaki et al., 2013), which is
101 also proposed for the modern TAG hydrothermal field (0.56–1.05; Brügmann et al.,
102 1998). In the Brooks Range belt, Re-Os data of 10 massive and vein pyrites from Red
103 Dog deposit yields an isochron age of 338.3 ± 5.8 Ma with an initial $^{187}Os/^{188}Os$ of
104 0.20 ± 0.21, which differs from the contemporaneous value (~1) of seawater (*pers.*
105 *comm.*, Slack, 2014; paper in review to SEG). This indicates that only crustal sources
106 older than ~ 410 Ma are unlikely to provide Os in the ore-forming hydrothermal fluids,
107 and that the unradiogenic value does not preclude a mantle-like source (Morelli et al.,
108 2004). In the Hokuroku District of Japan, sulfides from four Kuroko, three Oko and
109 one Keiko ores from the Kuroko ore deposits yield an isochron age of 14.32 ± 0.51
110 Ma, with an initial $^{187}Os/^{188}Os$ value of ~ 0.75 (Terakado, 2001a). This value is in the

range of the Miocene seawater $^{187}Os/^{188}Os$ value (0.73 to 0.85; Peucker-Ehrenbrink et al., 1995), suggesting that the Os of the Kuroko ore deposits in the northeast Japan was mainly derived from seawater (Terakado, 2001a). In the Wanibuchi Mine (yields an isochron age of 18.44 ± 0.60 Ma), the initial $^{187}Os/^{188}Os$ ratio (0.621 ± 0.013) might reflect the contemporaneous local seawater ratio (~0.57–0.66) that was more affected by Os derived from the volcanic activities of Japan Sea formation (Terakado, 2001b). In the late Triassic Gacun volcanogenic massive sulfide deposit, southwestern China, the Re-Os isotopic compositions of sulfide ores yield a 8-point isochron age of 217 ± 28 Ma, with an initial $^{187}Os/^{188}Os$ of 0.52 ± 0.73, suggesting a mixing of hydrothermal fluid and late Triassic seawater (Hou et al., 2003). The radiogenic Os compositions (0.566–1.054) of sulfide samples from the TAG hydrothermal field indicate that there is a variable mixing of ocean crust-derived Os and seawater Os, and this mixing is controlled by the redox conditions (Brügmann et al., 1998; Ravizza et al., 1996). Although the Re-Os isotopic composition of seafloor hydrothermal sulfides can provide important information on metal and fluid sources, mixing between hydrothermal fluid and seawater, and geochemical processes, little is known about the Re-Os isotopic composition of sulfides from seafloor hydrothermal systems in mid-ocean ridge (MOR) and back-arc basin (BAB), due to their low concentrations (Re < 0.2 ppb; Os < 2 ppt) in sulfides and the difficulty in obtaining pure sulfide samples (e.g. fine-grained intergrowth and the removal of other minerals such as sulfates and oxides). At present, analytical techniques developed by Birck et al. (1997) have allowed precise measurements of Os at a few tens of parts per trillion (ppt) levels,

enabling the analysis of more common sulfide samples (Gannoun et al., 2003).

In this study, Re-Os abundance and isotopic compositions have been measured, for the first time, in the seafloor massive sulfide samples from the EPR near 13°N and 1-2°S, MAR, CIR, SWIR and BAB (Fig. 1). We describe the characteristics of Re-Os abundance and isotopic composition in sulfides, in combination with major elements of sulfide samples, characterize the seawater Os contributions, attempt to understand the implications of initial $^{187}Os/^{188}Os$ for ancient seafloor hydrothermal sulfide deposits, reveal the enrichment condition of Re-Os, and evaluate the Os flux from hydrothermal fluid to seafloor hydrothermal precipitation.

2. Sampling and methods

In 2005, 2007, 2008, 2009, and 2010, during the DY105-17, DY115-19, DY115-20, and DY115-21 cruises of R/V *Dayang Yihao*, sulfide samples were recovered by TV-grab samplers from several sites. These included the fast-spreading EPR near 13°N; the ultra-fast spreading EPR near 1-2°S; the Kairei hydrothermal field (KHF) and Edmond hydrothermal field (EHF) on the intermediate-spreading CIR near 25°S; the A area on the ultra-slow spreading SWIR; and the LHF on the slow-spreading MAR. Sulfide samples from Sonne 99 hydrothermal field (S99HF) in the back-arc North Fiji Basin (NFB) were collected in 1998 during the SO134 curise of the R/V *Sonne* for the German HYFIFLUX II project (Fig. 1).

In the EPR near 13°N and 1-2°S, KHF, EHF, A area, and S99HF, the massive sulfide deposits are hosted by mid-ocean ridge basalts (MORBs). In the LHF, the massive sulfide deposit is associated with ultramafic rocks located in a debris flow consisting of heterogeneous ultramafic and mafic intrusive rocks, including serpentinized harzburgite, serpentinized dunite, gabbronorite, and olivine-bearing basalt (Petersen et al., 2009). Massive sulfide deposits include both focused high-temperature (> 300°C) fluid outflow through chimneys as well as low-temperature (< 200°C) fluids from mounds in the EPR near 13°N, KHF, EHF, LHF, and S99HF (Gallant and Von Damm, 2006; Koschinsky et al., 2002; Merlivat et al., 1987; Michard et al., 1984; Petersen et al., 2009). Table 1 and Fig. 2 contain information about the sampling location, depth, and mineralogy of the massive sulfide samples. Most massive sulfide samples indicating multi-stage deposition consist of major pyrite ± marcasite, chalcopyrite,

177 sphalerite, and minor barite, Pb-sulfide or galena.

178 Massive sulfide samples were carefully taken from distinct zones or representative
179 portions of the sulfides. All of the samples were crushed and sieved to select sulfide
180 grains between 50 μm and 2 mm, and then sulfides and some gangue minerals were
181 separated by ethanol elutriation. As most of the samples were fine-grained and
182 intergrown, we used an integrated mechanical separating method (including a
183 high-frequency dielectric splitter, a magnetic separator, and an electromagnetic
184 separator) to obtain ~200–500 mg of pure monomineralic or mineral aggregate
185 samples. All sulfide mineral samples for Re-Os analysis were then hand-picked
186 carefully under a binocular microscope to avoid sulfates and oxides. In oxidizing
187 conditions, Re is highly soluble (Crusius et al., 1996), and the seawater-derived
188 hydrogenous Os can be scavenged by Fe-oxides (Ravizza et al., 1996), and
189 Pierson-Wickmann et al. (2002) also showed that Os liberated during alteration was
190 partially re-precipitated in oxides, with Os isotope compositions very similar to those
191 of the original rocks. Whereas, a large amount of Re can be lost during alteration
192 processes (Peucker-Ehrenbrink and Hannigan, 2000). As such, it is possible that the
193 post-depositional oxidation can affect the Re and Os abundances and isotope
194 composition of primary sulfide (e.g. Brügmann et al., 1998; Gannoun et al., 2003;
195 Ravizza et al., 1996). As a result we took care to avoid the effects of oxidation.

196 These samples were divided into sub-samples, which were placed in distilled water,
197 exposed to ultrasonic waves for 15min, and then washed in de-ionised Milli-Q water
198 (18.2 MΩ) to remove impurities from the surface. The samples were dried at 65 and

105°C and then ground to < 63 μm.

221 *2.1. Fe, Cu, Pb and Zn determinations*

222 Exactly 40mg of the < 200 μm powders were weighed, then added to Teflon vials.
223 Next, 0.5 mL of 22.5 mol/L pure HF, 2 mL of 12 mol/L pure HCl were added in turn
224 and the samples were heated at 150°C for 24h in closed vials on an electrothermal
225 plate. After that, 0.6 mL of 16 mol/L pure HNO_3 was added and heated in closed vials
226 at 150°C for 12h. Then samples were dried until no white smoke was present. When
227 the samples were dry, 1mL of 16 mol/L pure HNO_3 and 1mL de-ionised Milli-Q water
228 (18.2 MΩ) were added to re-dissolve for 12h (Yin et al., 2011). All acids above are
229 MOS (Metal-Oxide-Semiconductor) pure grade. Finally, Fe, Cu, Pb, and Zn were
230 analyzed by IRIS Intrepid II XSP ICP-AES (Thermo Fisher Scientific) at Qingdao
231 Institute of Marine Geology, relative standard deviation (RSD) < 2%. The reference
232 materials GBW07267, GBW07268, GBW07270, and WMS-1A were run as external
233 standards to evaluate the accuracy.
234
235
236
237
238
239
240
241
242

243 *2.2. Rhenium-Osmium Analysis*

244 Rhenium and Os abundance and isotope analyses were performed in the TOTAL
245 Laboratory for Source Rock Geochronology and Geochemistry (a member of the
246 Durham Geochemistry Centre) at Durham University, following standard protocols
247 (Selby et al., 2009). In brief, rhenium and osmium were purified from the sulfide
248 samples (~400 mg) using carius tube digestion with HCL-HNO_3 medium, with the Os
249 isolated and purified using solvent extraction and micro-distillation. Rhenium was
250 separated using anion chromatography. Isotope ratios of Re and Os were determined
251 using negative thermal ionization mass spectrometry on a Thermo Fisher Scientific
252 TRITON mass spectrometer. Analytical blanks (2.5 ± 0.06 pg and 0.2 ± 0.1 pg; 1σ, *n*
253 = 3; respectively for Re and Os, with an average $^{187}Os/^{188}Os$ ratio of 0.25 ± 0.03) and
254 results for standard in-house solutions run during this study are identical to those
255 previously published ($^{185}Re/^{187}Re$ = 0.598251 ± 0.001510, 1σ S.D., *n* = 13;
256 $^{187}Os/^{188}Os$ ratio 0.160912 ± 0.000559, 1σ, *n* = 13) (Nowell et al., 2008; Selby et al.,
257 2009). Uncertainties for $^{187}Re/^{188}Os$ and $^{187}Os/^{188}Os$ are determined by full error
258 propagation of uncertainties in Re and Os mass spectrometer measurements, blank
259 abundances and isotopic compositions, spike calibrations and reproducibility of
260 standard Re and Os isotopic values.
261
262
263
264

3. Results

3.1. Re and Os concentrations in sulfides

Rhenium and Os concentrations and isotopic data are shown in Table 2. Massive sulfides from the EPR near 13°N and 1-2°S, MAR, CIR, SWIR, and BAB have Os concentrations between 1.7 and 79.9 ppt and Re concentrations between 0.10 and 73.60 ppb (Table 2; Figs. 3a, 3b). The Re concentrations in the S99HF are variable (0.10 to 73.60 ppb), and show the largest range, which exhibit two highest concentrations (44.45 and 73.60 ppb) and one lowest concentration (0.10 ppb) in the massive sulfide samples (Table 2). The Os concentrations of sulfide samples from the EHF is significantly more variable (1.7 to 79.9 ppt) than that of sulfide samples from the other hydrothermal fields, if we exclude the three samples (IR05-TVG12-8-2, IR05-TVG13-9.2-1, and 19III-S18-TVG9), the remaining samples do not exhibit much variability (1.7 to 8.84 ppt) (Table 2). The Os concentrations of sulfide samples from the EPR near 13°N consist also a large range (5.74 to 53.36 ppt). Further, Re concentrations of pyrite and Fe-Cu sulfide mineral aggregate samples are usually higher than that of sphalerite or Zn-enriched sulfide mineral aggregates in massive sulfide samples (Table 1, 2; Fig. 4a). The overall ranges in Os contents in massive sulfide samples from the EPR near 13°N and 1-2°S, LHF, EHF, KHF, A area, and NFB are roughly similar (Table 2; Fig. 3a).

287 *3.2. Re-Os isotopic compositions of the sulfides*

288 The measured $^{187}Os/^{188}Os$ value in the sulfide samples varied from 0.645 to 1.209
289 (Table 2), with no relationship shown between $^{187}Os/^{188}Os$ ratio and mineral aggregate
290 type (e.g. Fe-sulfide, Fe-Cu sulfide, Zn-rich sulfide) (Fig. 4c). The $^{187}Os/^{188}Os$ ratios
291 of all samples are significantly more radiogenic than that of MORB (Fig. 3c). Most of
292 the $^{187}Os/^{188}Os$ ratios agree with or are slightly less radiogenic than the value for
293 modern seawater (~1.06), which is similar to that estimated for seawater ~2 ka
294 (Peucker-Ehrenbrink and Ravizza, 2000) (Fig. 3c). Only two samples possess
295 $^{187}Os/^{188}Os$ ratios that are significantly lower than that of seawater (0.645 ± 0.066,
296 MAR05-TVG1-10-2, and 0.730 ± 0.066, MAR05-TVG1-21 from the LHF, MAR)
297 (Fig. 3c).

298 The sulfide samples have a significantly large range of $^{187}Re/^{188}Os$ ratios (from 64 to
299 100,334) (Fig. 3d), although ^{187}Os ingrowth could change the $^{187}Os/^{188}Os$ ratios of the
300 sulfide samples during a relatively short interval of time (Brügmann et al., 1998), the
301 young age (e.g. 1,900–2,100 yr, sulfides of the EPR near 13°N; Lalou et al., 1985) of
302 sulfides precludes any notable ^{187}Os ingrowth despite the large $^{187}Re/^{188}Os$ ratios (e.g.
303 sample EPR05-TVG2-1-1 and EPR05-TVG2-1-6). The rather constant $^{187}Os/^{188}Os$
304 values in most samples with very different Re/Os ratios also show insignificant ^{187}Os
305 ingrowth (Brügmann et al., 1998; Table 2). For example, for the most Re enriched
306 sample (42GTV-3, 73.6 ppb Re) only 1.8 ppq ^{187}Os would be generated in ~2 ka. In
307 addition, $^{187}Re/^{188}Os$ ratios of pyrite and Fe-Cu sulfide mineral aggregates in the
308 massive sulfide samples are usually higher than that of sphalerite or Zn-enriched

sulfide mineral aggregate samples (Fig. 4d).

4. Discussion

4.1. Seawater osmium contributions

It is known that the Os isotopic composition of MORB is about 0.133 (Gannoun et al., 2007; Schiano et al., 1997), and is about 0.121 in abyssal peridotite (Harvey et al., 2006; Snow et al., 1995). The $^{187}Os/^{188}Os$ ratios of hydrothermal fluids from the Juan de Fuca Ridge are from ~0.110 to 1.04 (Sharma et al., 2000, 2007), which are between MORB (~0.133) and seawater (~1.06). The Os isotopic ratio of present-day and ~ 2 ka seawater is radiogenic (~ 1.0; Peucker-Ehrenbrink and Ravizza, 2000), significantly different from unradiogenic Os isotopic compositions of MORB and ultramafic rocks (e.g. Roy-Barman and Allègre, 1994). Therefore, the Os isotopic compositions of massive sulfides can be used as evidence for the source of osmium and by inference the associated metals (Fe, Cu, Zn) as well as the physicochemical processes involved during metal mobilization (Brügmann et al., 1998).

The majority of the $^{187}Os/^{188}Os$ values for the massive sulfide samples fall in a narrow range (0.968–1.209) (Fig. 3c, 5), that are close to or within uncertainty of the modern seawater $^{187}Os/^{188}Os$ value (~ 1.06; Peucker-Ehrenbrink and Ravizza, 2000), and significantly more radiogenic than that of MORB (Fig. 3c, 5). All the Os isotopic data in sulfide samples from the EPR near 13°N and 1-2°S, KHF, EHF, A area, and S99HF indicates that the Os is mainly derived from seawater (Fig. 5b), which can be interpreted as evidence of entrainment of seawater into hydrothermal fluids (e.g. Ravizza et al., 1996; Roy-Barman and Allègre, 1994).

In the ancient VMS deposits, initial $^{187}Os/^{188}Os$ isotope compositions vary greatly

353 even in the same deposit. Take the Iberian Pyrite Belt for example, initial osmium
354 isotope ratios of pyrites in sulfide-rich stockwork ores are from 0.451 to 1.08, much
355 lower than those in pyrites from cassiterite-rich stockwork ores (4.89 to 7.85), and let
356 alone massive copper-tin ores (0.376 to 14.1) (Mathur et al., 1999; Munhá et al.,
357 2005). The high initial $^{187}Os/^{188}Os$ ratios were interpreted to be affected by late
358 hydrothermal and Variscan metamorphic isotope disturbances (Munhá et al., 2005),
359 making the ratios inappropriate for tracing of the ancient contemporaneous seawater
360 composition. However, the initial $^{187}Os/^{188}Os$ ratio (0.49 ± 0.07) of Neves-Corvo
361 sulfide-rich stockwork ores in the Iberian Pyrite Belt, obtained according to best-fit
362 calculations on the isochron (358 ± 29 Ma) (Munhá et al., 2005) is nearly identical to
363 that inferred for Late Devonian (358 ± 9 Ma) seawater (~ 0.3–0.7; Harris et al., 2013).
364 Further, the Os isotopic composition of Middle Devonian Givetian (~385 Ma)
365 seawater is estimated to be the same as the initial Os isotopic ratio of Devonian
366 seafloor metalliferous sediments ($^{187}Os/^{188}Os$ ~ 0.17–0.2) in the Southern Urals,
367 which is associated with Alexandrinka sulfide deposit (Harris et al., 2013; Tessalina et
368 al., 2008). In the Sanbagawa metamorphic belt, the Re-Os isotopic compositions of
369 massive sulfides from the Iimori Besshi-type deposit, yield a model isochron age
370 (148.4 ± 1.4 Ma) and an initial $^{187}Os/^{188}Os$ of 0.41 ± 0.14 (Nozaki et al., 2013), which
371 is similar to the $^{187}Os/^{188}Os$ ratios of ancient seawater which recorded by the
372 individual organic-rich mudstones (ancient seawater age 155 ± 4.3 Ma, initial
373 $^{187}Os/^{188}Os$ of 0.59 ± 0.07; Cohen et al., 1999), suggesting that these ancient sulfide
374 deposits were formed by the mixing process between ancient seawater and

hydrothermal fluid, and their initial $^{187}Os/^{188}Os$ ratios were not altered by later hydrothermal fluids or metamorphism after a long geologic period. If it is true, the initial Os isotopic ratios of ancient sulfide deposits can be used in discussion of the origin of Os and by inference the associated metals.

The Os isotope composition of seawater has varied through time (Peucker-Ehrenbrink and Ravizza, 2012). Although the Paleozoic record is poorly established, the Cenozoic record shows a progressive trend towards radiogenic values. If seafloor sulfides predominantly record seawater values of Os then this proposes that ancient deposits will have variable Os.

In addition, Os isotopic compositions of at last two samples (0.645 ± 0.066, MAR05-TVG1-10-2, and 0.730 ± 0.066, MAR05-TVG1-21) from the LHF in the MAR are less radiogenic than that of ambient seawater, suggesting it is likely to have been influenced by both radiogenic Os from seawater and unradiogenic Os released by alteration of the MORB and/or the ultramafic rocks (Fig. 5a). According to the mixing trajectories calculated using the method outlined by Langmuir et al. (1978), the mixing curve between the MORBs end member (Os concentration 13.26 ppt, $^{187}Os/^{188}Os$ ratio 0.136; Gannoun et al., 2007; Schiano et al., 1997), which are usually considered as the source component of seafloor hydrothermal fluid and seawater (Os concentration 0.01 ppt, $^{187}Os/^{188}Os$ ratio 1.06; Peucker-Ehrenbrink and Ravizza, 2000) fits most of the Os data points of massive sulfide samples, with $r_{SB} = 0.1$ (Fig. 5b). Further, the less radiogenic $^{187}Os/^{188}Os$ ratios (e.g. sample MAR05-TVG1-10-2 and MAR05-TVG1-21) indicate that Os derived from alteration of the oceanic crust is

397 released to hydrothermal fluid in association with mixing process between seawater
398 and fluid (Brügmann et al., 1998; Ravizza et al., 1996), which can be taken place both
399 at vent site and in the sub-seafloor where seawater commonly is entrained within
400 pre-existing sulfide deposit (e.g. hydrothermal mounds, layers, lenses, feeder zones,
401 etc.) (e.g. Rona and Scott, 1993; Zierenberg et al., 1998), and comparing to other
402 sulfides (e.g. EPR near 1-2°S, KHF, S99HF), reflect a relative less proportion of
403 seawater component incorporated into these sulfides during mixing between seawater
404 and hydrothermal fluid.
405
406
407
408
409
410
411
412
413
414
415
416
417
418

419 *4.2. Re-Os enrichment*

420 Rhenium concentrations of this study are partly lower (0.1 to 73.60 ppb) than that of
421 sulfides from the Iimori Besshi-type massive sulfide deposit (24 to 300 ppb; Nozaki et
422 al., 2010), the Alexandrinka ancient seafloor hydrothermal system (11 to 31 ppb;
423 Tessalina et al., 2008), the Dergamish massive sulfide deposits (6 to 41 ppb; Gannoun
424 et al., 2003), and the Red Dog deposit (0.644 to 383 ppb; Morelli et al., 2004), but
425 similar to those of massive sulfides from the TAG hydrothermal field (2 to > 70 ppb;
426 Brügmann et al., 1998) and the Ivanovka massive sulfide deposits (0.18 to 6 ppb;
427 Gannoun et al., 2003). The variation in Re content reflects changing temperature, pH,
428 redox conditions and complexing behavior of the hydrothermal fluids, Re is highly
429 soluble in seawater oxidizing conditions (larger amounts of seawater mixing with
430 hydrothermal fluid could cause more oxidized conditions), leading to low Re
431 concentrations in sulfide, whereas under hydrothermal fluid reducing conditions it is
432 less mobile and becomes concentrated in sulfide (e.g. Brügmann et al., 1998; Keppler,
433 1996; Xiong and Wood, 1999).

434 The Os concentrations in massive sulfide samples of this study are general higher (1.7
435 to 79.9 ppt) than that of massive sulfides from the TAG hydrothermal field (0.04–4.20
436 ppt; Brügmann et al., 1998). In comparison to ancient massive sulfides, the Os
437 abundances of sulfides from this study are typically lower than that of the Iimori
438 Besshi-type massive sulfide deposit (224 to 660 ppt; Nozaki et al., 2010), the
439 Alexandrinka ancient seafloor hydrothermal system (69 to 1,071 ppt; Tessalina et al.,
440 2008), the Dergamish and Ivanovka massive sulfide deposits (18 to 2,463 ppt;

441 Gannoun et al., 2003), and the Red Dog deposit (14 to 3,353 ppt; Morelli et al., 2004).
442 Because of the great mobility of Os in the high-temperature hydrothermal system
443 (Brügmann et al., 1998), Os concentrations in sulfide samples from the EPR near
444 13°N and 1-2°S, MAR, CIR, SWIR, and BAB are general higher than that of the
445 massive sulfides from the TAG hydrothermal field, suggesting the formation
446 temperatures of these sulfides are relatively lower than that of the sulfides from the
447 TAG hydrothermal field (> 300°C; Chiba et al., 2001).
448 In many submarine hydrothermal systems, low-temperature (< 200 °C), diffusely
449 venting sulfide chimneys are common (e.g. Ames et al., 1993). Sulfide assemblages
450 which were formed at different temperatures have distinct major and trace element
451 compositions, such as Pb, which is enriched in the minor of invisible galena, Pb-As
452 sulfosalts in massive sulfide samples (see Fig. 2), is usually precipitated in the
453 low-temperature, slightly oxidizing conditions during the late or the waning stage of
454 hydrothermal activity (e.g. Fouquet et al., 1996; Kim et al., 2006; Kristall et al., 2006),
455 and are attributed to the weaker HS^- complexation at lower temperature (Hannington
456 et al., 1991). The Os/Re ratios of massive sulfides show positive correlations (R^2 =
457 0.67, $p < 0.01$, $n = 11$) with Pb (up to 0.15 wt.% concentrations) in the EHF (Fig. 6a),
458 which might also indicate Os incorporated into sulfides under lower temperature
459 conditions, possibly less than 200 °C (Hannington et al., 1991).
460 In massive sulfide samples, very low Re content (< 1 ppb) showed positive correlation
461 with Fe. High Re content (> 10 ppb) showed negative correlation with Fe (Fig. 6b),
462 implying that the Re enrichment is not related to the Fe content of massive sulfides.

Some high-Fe samples (e.g. sample 19III-S18-TVG9, Fe content 43.8 %, and sample IR05-TVG13-9.1, Fe content 38.4 %) had the highest Os content (79.9 ppt) and some had the lowest Os content (1.7 ppt) (see Table 2). This tends to imply, judging from these samples, that the Os contents of these massive sulfides are not primarily controlled by the Fe content. Massive sulfide samples with very low Re contents (< 0.2 ppb) have very low Cu contents. Samples with intermediate Re contents (0.2 to 5 ppb) have a wide range of Cu content. Samples with high Re contents (> 5 ppb) also show a significant range of Cu content (Fig. 6c). On the other hand, massive sulfide samples with lower Re concentration usually have higher Zn concentration (Fig. 6d), and Os/Re ratios are high in the Zn-enriched sulfide mineral aggregate samples (e.g. sample 26.1GTV-1, IR05-TVG12-8-3 and IR05-TVG12-14). This also indicates that Re is less compatible than Os in sphalerite or Zn-enriched sulfide mineral aggregate samples, and together these suggest that the Re-Os enrichment is not related to Zn-enriched sulfide mineral facies. This phenomenon is also observed in ancient VMS deposit such as the Red Dog deposit with the higher Re and Os content of pyrite than sphalerite in the massive sulfides (Morelli et al., 2004).

In addition, the high Os contents of sulfides from the Alexandrinka, the Dergamish and Ivanovka massive sulfide deposits in island-arc environment show that the ^{187}Os enrichment of the sulfides from ^{187}Re decay (Brügmann et al., 1998; Tessalina et al., 2008), and the estimated minimal Os contents of Devonian fluid (20 ppt; Tessalina et al., 2008) are three orders of magnitude higher than that ($1.9–98\times10^{-3}$ ppt; Sharma et al., 2000, 2007) of the hydrothermal fluid from the Juan de Fuca Ridge in mid-ocean

485 ridge setting, suggesting that seafloor hydrothermal massive sulfides from MOR (e.g.
486 EPR near 13°N and 1-2°S, CIR, and MAR) are characterized by low Os
487 concentrations compared with island-arc hosted VHMS deposits (e.g. Urals, Iberian
488 pyrite belt; Tessalina et al., 2008). In contrast to the seafloor hydrothermal massive
489 sulfides (Fig. 3a, 3b), the MORBs are depleted in Re and Os which might explain the
490 higher $^{187}Re/^{188}Os$ ratios of the sulfides from the EPR near 1-2°S and the KHF, since
491 an increasing $^{187}Re/^{188}Os$ ratio shows the interaction of oxidized seawater and reduced
492 hydrothermal fluid. The higher Os and Re concentrations in these samples may reflect
493 that Os and Re were concentrated in the fluid, Os and Re behaves as a highly mobile
494 element during basalt-fluid interaction (Brügmann et al., 1998).
495
496
497
498
499
500
501
502
503
504
505
506

507 *4.3. Re-Os Flux*

508 These modern massive sulfide sample analyses allow a meaningful estimate of the
509 magnitude of the hydrothermal Re and Os flux. We present a simple calculation below
510 the premise that vent fluids can readily supply Re and Os with the $^{187}Os/^{188}Os$ ratio
511 near the present-day seawater (~ 1.06) to the massive sulfides. The amount of seafloor
512 massive sulfide deposits in the global oceans has been estimated by using new deposit
513 occurrence data from 10,000 km of ridge, arc, and back-arc spreading centers, which
514 is on the order of 6×10^8 tonnes, containing about 3×10^7 tonnes of copper and zinc
515 (Hannington et al., 2011). The method to roughly estimate the seafloor massive
516 sulfide sink for Re and Os:

517 $S_{Re} = M_{sulfide} \times X_{Re}$……..(1)

518 $S_{Os} = M_{sulfide} \times X_{Os}$……..(2)

519 where S_{Re} and S_{Os} are the soluble Re and Os from hydrothermal fluids supplied to the
520 massive sulfide deposits; $M_{sulfide}$ is the total mass of seafloor massive sulfide deposits,
521 as above; and X_{Re} and X_{Os} are the Re and Os contents in the massive sulfide. Based on
522 analyses of Re (0.1–73.60 ppb) and Os (1.7–79.9 ppt) in seafloor massive sulfides
523 from the EPR near 13°N and 1-2°S, MAR, CIR, SWIR, and BAB, it is estimated that
524 roughly 0.6 to 44 tonnes (avg 4 tonnes, n = 38) of solube Re and 1 to 48 kg (avg 8 kg,
525 n = 38) of soluble Os from hydrothermal fluids is supplied to the sulfide deposits.
526 In addition, Os enrichment of seafloor massive sulfide samples from the EPR near
527 13°N and 1-2°S, LHF, KHF, EHF, A area, and S99HF is occurring under
528 low-temperature hydrothermal fluid conditions. On the mid-ocean ridges, the mass of

hydrothermal fluid heated to low-temperatures (< 350 °C) is on the order of 6–12 $\times 10^{13}$ kg/yr (Elderfield and Schultz, 1996). Assuming Os concentration of 98 pg/kg in the low-temperature fluids as suggested by Sharma et al. (2000), the global flux of Os to low-temperature hydrothermal vents is about 5–11 kg per year, far less than the 100 kg per year estimated by Ravizza et al. (1996). On these figures, it is seen that in just several years, low-temperature vents at the mid-ocean ridges alone transport more Os to the oceans than is estimated to occur in all of the seafloor low-temperature hydrothermal sulfide deposits from the ocean ridges, arcs and back-arc basins. The fate of the excess Os is unclear, but it has long been known that distal marine sediments, Fe-Mn crusts and nodules are enriched in Os deposited from plumes associated with mid-ocean ridge hydrothermal systems (Burton et al., 1999; Palmer and Turekian, 1986; Ravizza and McMurtry, 1993; Ravizza et al., 1996). This plume fallout does not form seafloor hydrothermal sulfide deposits, and may account for a large fraction of the missing Os.

5. Conclusions

The study of Re-Os systematics of seafloor massive sulfide from the MORs and BAB indicates that the Re concentrations range from 0.1 to 73.6 ppb, Os concentrations are very low, range from 1.7 to 79.9 ppt, and mainly derived from seawater. Two samples from the LHF have shown that Os content and isotopic compositions are controlled by the extent of mixing between hydrothermal fluid and seawater. Since the Os in most of the modern seafloor massive sulfide samples being predominantly derived from seawater, it is possible that the initial Os of ancient seafloor sulfide deposits may be also from ancient seawater. Therefore, the initial $^{187}Os/^{188}Os$ isotopic ratio of sulfide may be useful in discussions of the composition of ancient seawater. Also, the Re-Os isotopic systematics may be useful in speculation about the similarity between ancient sulfide deposit and modern seafloor hydrothermal deposit.

The enrichment of Os in these seafloor massive sulfides is consistently related to low-temperature (< 200°C) venting. The massive sulfide samples with lower Re contents and higher Os/Re ratios usually have higher Zn contents, indicating that Re is less compatible than Os in sphalerite or Zn-enriched sulfide mineral aggregates. It is estimated that the seafloor massive sulfide deposits contain a total of roughly 0.6–44 tonnes of Re and 1–48 kg of Os. This implies that it is unlikely that a large Re-Os-type massive sulfide deposit will be discovered in the ocean. In addition, the global flux of Os to low-temperature hydrothermal vents is up to 11 kg per year, it seems probable that the excess Os becomes associated with sediments, Fe-Mn crusts and nodules distal from the hydrothermal vents.

Acknowledgements

We would like to thank the crews during the DY105-17, DY115-19, DY115-20, and DY115-21 cruises for helping us collect samples. We are grateful to Dr. Erio Rahders of Institute for Geological Sciences, Geology Department, Free University of Berlin, Dr. Xiguang Deng of Guangzhou Marine Geological Survey, China Geological Survey, and Dr. Huaiming Li of Second Institute of Oceanography, SOA, China for providing some of the samples. We are most grateful for the detailed and constructive comments and suggestions provided by Dr. John F. Slack, Dr. Tatsuo Nozaki and one anonymous reviewer, which greatly improved an earlier version of the manuscript. This work was supported by National Key Basic Research Program of China (Grant No. 2013CB429700), National Special Fund for the 12th Five Year Plan of COMRA (Grant No. DY125-12-R-02, DY125-11-R-05), National Natural Science Foundation of China (Grant No. 41325021, 40830849, 40976027), Strategic Priority Research Program of the Chinese Academy of Sciences (Grant No. XDA11030302), and Shandong Province Natural Science Foundation of China for Distinguished Young Scholars (Grant No. JQ200913).

595 **References**

596 Ames, D.E., Franklin, J.M., Hannington, M.D., 1993. Mineralogy and geochemistry
597 of active and inactive chimneys and massive sulfide, Middle Valley, northern
598 Juan de Fuca Ridge: An evolving hydrothermal system. Can. Mineral. 31,
599 997–1024.

600 Baker, E.T., German, C.R., 2004. On the global distribution of mid-ocean ridge
601 hydrothermal vent-fields. Amer. Geophys. Union, Geophys. Monogr. 148, pp.
602 245–266.

603 Birck, J.-L., Roy-Barman, M., Capmas, F., 1997. Re-Os isotopic measurements at
604 femtomole level in natural samples. Geostand. Newsl. 20, 19–27.

605 Brügmann, G.E., Birck, J.L., Herzig, P.M., Hofmann, A.W., 1998. Os isotopic
606 composition and Os and Re distribution in the active mound of the TAG
607 hydrothermal system, Mid-Atlantic Ridge. Proc. ODP, Sci. Res. 158, 91–100.

608 Burton, K.W., Bourdon, B., Birck, J.-L., Allègre, C.J., 1999. Osmium isotope
609 variations in the oceans recorded by Fe-Mn crusts. Earth Planet. Sci. Lett. 171,
610 185–197.

611 Chiba, H., Masuda, H., Lee, S.-Y., Fujioka, K., 2001. Chemistry of hydrothermal
612 fluids at the TAG active mound, MAR 26°N, in 1998. Geophys. Res. Lett. 28,
613 2919–2922.

614 Cohen, A.S., Coe, A.J., Bartlett, J.M., Hawkesworth, C.J., 1999. Precise Re-Os ages
615 of organic-rich mudrocks and the Os isotopic composition of Jurassic seawater.
616 Earth Planet. Sci. Lett. 167, 159–173.

617 Crusius, J., Calvert, S., Pedersen, T., Sage, D., 1996. Rhenium and molybdenum
618 enrichment in sediments as indicators of oxic, suboxic and sulfidic conditions of
619 deposition. Earth Planet. Sci. Lett. 145, 65–78.
620 Elderfield, H., Schultz, A., 1996. Mid-ocean ridge hydrothermal fluxes and the
621 chemical composition of the ocean. Annu. Rev. Earth Planet. Sci. 24, 191–224.
622 Fouquet, Y., Knott, R., Cambon, P., Fallick, A., Rickard, D., Desbruyeres, D., 1996.
623 Formation of large sulfide mineral deposits along fast spreading ridges.
624 Example from off-axial deposits at 12°43'N on the East Pacific Rise. Earth
625 Planet. Sci. Lett. 144, 147–162.
626 Fouquet, Y., 1997. Where are the large hydrothermal sulphide deposits in the oceans?
627 Phil. Trans. R. Soc. Lond. A 355, 427–441.
628 Gallant, R.M., Von Damm, K.L., 2006. Geochemical controls on hydrothermal fluids
629 from the Kairei and Edmond vent fields, 23°–25°S, Central Indian Ridge.
630 Geochem. Geophys. Geosyst. 7, Q06018, doi:10.1029/2005GC001067.
631 Gannoun, A., Tessalina, S., Bourdon, B., Orgeval, J.-J., Birck, J.-L., Allègre, C.-J.,
632 2003. Re-Os isotopic constraints on the genesis and evolution of the Dergamish
633 and Ivanovka Cu (Co, Au) massive sulphide deposits, south Urals, Russia.
634 Chem. Geol. 196, 193–207.
635 Gannoun, A., Burton, K.W., Parkinson, I.J., Alard, O., Schiano, P., Thomas, L.E.,
636 2007. The scale and origin of the osmium isotope variations in mid-ocean ridge
637 basalts. Earth Planet. Sci. Lett. 259, 541–556.
638 Hannington, M., Herzig, P., Scott, S., Thompson, G., Rona, P., 1991. Comparative

mineralogy and geochemistry of gold-bearing sulfide deposits on the mid-ocean ridges. Mar. Geol. 101, 217–248.

Hannington, M.D., Jonasson, I.R., Herzig, P.M., Petersen, S., 1995. Physical and chemical processes of seafloor mineralization at mid-ocean ridges. In Humphris, S.E., Zierenberg, R.A., Mullineaux, L.S., Thomson, R.E., (eds.), Seafloor Hydrothermal Systems: Physical, Chemical, Biological and Geological Interactions, Amer. Geophys. Union, Geophys. Monogr. 91, pp. 115–157.

Hannington, M., Jamieson, J., Monecke, T., Petersen, S., Beaulieu, S., 2011. The abundance of seafloor massive sulfide deposits. Geology 39, 1155–1158.

Harris, N.B., Mnich, C.A., Selby, D., Korn, D., 2013. Minor and trace element and Re-Os chemistry of the upper Devonian Woodford shale, Permian basin, west Texas: Insights into metal abundance and basin processes. Chem. Geol., 356, 76–93. http://dx.doi.org/10.1016/j.chemgeo.2013.07.018.

Harvey, J., Gannoun, A., Burton, K.W., Rogers, N.W., Alard, O., Parkinson, I.J., 2006. Ancient melt extraction from the oceanic upper mantle revealed by Re-Os isotopes in abyssal peridotites from the Mid-Atlantic ridge. Earth Planet. Sci. Lett. 244, 606–621.

Hou, Z.-Q., Wang, S.-X., Du, A.-D., Qu, X.-M., Sun, W.-D., 2003. Re-Os dating of sulfides from the volcanogenic massive sulfide deposit at Gacun, Southwestern China. Resour. Geol. 53, 305–310.

Kim, J., Lee, I., Halbach, P., Lee, K.-Y., Ko, Y.-T., Kim, K.-H., 2006. Formation of hydrothermal vents in the North Fiji Basin: Sulfur and lead isotope constraints.

Chem. Geol. 233, 257–275.

Keppler, H., 1996. Constraints from partitioning experiments on the composition of subduction zone fluids. Nature 380, 237–240.

Koschinsky, A., Seifert, R., Halbach, P., Bau, M., Brasse, S., De Carvalho, L.M., Fonseca, N.M., 2002. Geochemistry of diffuse low-temperature hydrothermal fluids in the North Fiji Basin. Geochim. Cosmochim. Acta 66, 1409–1427.

Kristall, B., Kelly, D.S., Hannington, M.D., Delaney, J.R., 2006. Growth history of a diffusely venting sulfide structure from the Juan de Fuca Ridge: A petrological and geochemical study. Geochem. Geophys. Geosyst. 7, Q07001, doi:10.1029/2005GC001166.

Lalou, C., Brichet, E., Hekinian, R., 1985. Age dating of sulfide deposits from axial and off axial structures of the East Pacific Rise near 12°50´N. Earth Planet. Sci. Lett. 75, 59–71.

Langmuir, C.H., Vocke, R.D.Jr., Hanson, G.N., 1978. A general mixing equation with applications to Icelandic basalts. Earth Planet. Sci. Lett. 37, 380–392.

Mathur, R., Ruiz, J., Tornos, F., 1999. Age and sources of the ore at Tharsis and Rio Tinto, Iberian Pyrite Belt, from Re-Os isotopes. Miner. Deposita 34, 790–793.

Merlivat, L., Pineau, F., Javoy, M., 1987. Hydrothermal vent waters at 13°N on the East Pacific Rise: isotopic composition and gas concentration. Earth Planet. Sci. Lett. 84, 100–108.

Michard, G., Albarède, F., Michard, A., Minster, J.-F., Charlou, J.-J., Tan, N., 1984. Chemistry of solutions from the 13°N East Pacific Rise hydrothermal site. Earth

683 Planet. Sci. Lett. 67, 297–307.
684 Morelli, R.M., Creaser, R.A., Selby, D., Kelley, K.D., Leach, D.L., King, A.R., 2004.
685 Re-Os sulfide geochronology of the Red Dog sediment-hosted Zn-Pb-Ag
686 deposit, Brooks range, Alaska. Econ. Geol. 99, 1569–1576.
687 Munhá, J., Relvas, J.M.R.S., Barriga, F.J.A.S., Conceição, P., Jorge, R.C.G.S., Mathur,
688 R., Ruiz, J., Tassinari, C.C.G., 2005. Osmium isotope systematics in the Iberian
689 Pyrite Belt. In: Mao, J., Bierlein, F. (Eds.), Mineral Deposit Research: Meeting
690 the Global Challenge, Springer Berlin Heidelberg, pp. 663–666.
691 Nowell, G.M., Luguet, A., Pearson, D.G., Horstwood, M.A., 2008. Precise and
692 accurate $^{186}Os/^{188}Os$ and $^{187}Os/^{188}Os$ measurements by Multi- Collector Plasma
693 Ionisation Mass Spectrometry (MC-ICP-MS) part I: solution analyses. Chem.
694 Geol. 248, 363–393.
695 Nozaki, T., Kato, Y., Suzuki, K., 2010. Re-Os geochronology of the Iimori
696 Besshi-type massive sulfide deposit in the Sanbagawa metamorphic belt, Japan.
697 Geochim. Cosmochim. Acta 74, 4322–4331.
698 Nozaki, T., Kato, Y., Suzuki, K., 2013. Late Jurassic ocean anoxic event: evidence
699 from voluminous sulphide deposition and preservation in the Panthalassa. Sci.
700 Rep. 3, 1889, doi:10.1038/srep01889.
701 Palmer, M.R., Turekian, K.K., 1986. $^{187}Os/^{186}Os$ in marine manganese nodules and the
702 constraints on the crustal geochemistries of rhenium and osmium. Nature 319,
703 216–220.
704 Petersen, S., Kuhn, K., Kuhn, T., Augustin, N., Hékinian, R., Franz, L., Borowski, C.,

2009. The geological setting of the ultramafic-hosted Logatchev hydrothermal field (14°45´N, Mid-Atlantic Ridge) and its influence on massive sulfide formation. Lithos 112, 40–56.

Peucker-Ehrenbrink, B., Ravizza, G., Hofmann, A.W., 1995. The marine $^{187}Os/^{186}Os$ record of the past 80 million years. Earth Planet. Sci. Lett. 130, 155–167.

Peucker-Ehrenbrink, B., Hannigan, R.E., 2000. Effects of black shale weathering on the mobility of rhenium and platinum group elements. Geology 28, 475–478.

Peucker-Ehrenbrink, B., Ravizza, G., 2000. The marine osmium isotope record. Terra Nova 12, 205–219.

Peucker-Ehrenbrink, B., Ravizza, G., 2012. Chapter 8 - Osmium Isotope Stratigraphy. The Geologic Time Scale, Boston, 145 – 166. http://dx.doi.org/10.1016/B978-0-444-59425-9.00008-1.

Pierson-Wickmann, A.C., Reisberg, L., France-Lanord, C., 2002. Behavior of Re and Os during low-temperature alteration: Results from Himalayan soils and altered black shales. Geochim. Cosmochim. Acta 66, 1539–1548.

Ravizza, G., McMurtry, G.M., 1993. Osmium isotopic variations in metalliferous sediments from the East Pacific Rise and the Bauer Basin. Geochim. Cosmochim. Acta 57, 4301–4310.

Ravizza, G., Martin, C.E., German, C.R., Thompson, G., 1996. Os isotopes as tracers in seafloor hydrothermal systems: metalliferous deposits from the TAG hydrothermal area, 26°N Mid-Atlantic Ridge. Earth Planet. Sci. Lett. 138, 105–119.

727 Rona. P.A., Scott, S.D., 1993.Seafloor hydrothermal mineralization: New perspective.
728 Econ. Geol. 88, 1935–1976.
729 Rona, P.A., 2003. Resources of the sea floor. Science 299, 673–674.
730 Roy-Barman, M., Allègre, C.J., 1994. $^{187}Os/^{186}Os$ ratios of mid-ocean ridge basalts
731 and abyssal peridotites. Geochim. Cosmochim. Acta 58, 5043–5054.
732 Schiano, P., Birck, J.L., Allègre, C.J., 1997. Osmium-strontium-neodymium-lead
733 isotopic covariations in mid-ocean ridge basalt glasses and the heterogeneity of
734 the upper mantle. Earth Planet. Sci. Lett. 150, 363–379.
735 Selby, D., Kelley, K.D., Hitzman, M.W., Zieg, J., 2009. Re-Os sulfide (bornite,
736 chalcopyrite and pyrite) systematics of the carbonate-hosted copper deposits at
737 Ruby Creek, southern Brooks Range, Alaska. Econ. Geol. 104, 437–444.
738 Sharma, M., Wasserburg, G.J., Hofmann, A.W., Butterfield, D.A., 2000. Osmium
739 isotopes in hydrothermal fluids from the Juan de Fuca Ridge. Earth Planet. Sci.
740 Lett. 179, 139–152.
741 Sharma, M., Rosenberg, E.J., Butterfield, D.A., 2007. Search for the proverbial
742 mantle osmium sources to the oceans: Hydrothermal alteration of mid-ocean
743 ridge basalt. Geochim. Cosmochim. Acta 71, 4655–4667.
744 Shirey, S.B., Walker, R.J., 1998. The Re-Os isotope system in cosmochemistry and
745 high-temperature geochemistry. Annu. Rev. Earth Planet. Sci. 26, 423–500.
746 Snow, J.E., Reisberg, L., 1995. Os isotopic systematics of the MORB mantle: results
747 from altered abyssal peridotites. Earth Planet. Sci. Lett. 133, 411–421.
748 Terakado, Y., 2001a. Re-Os dating of the Kuroko ore deposits from the Hokuroku

district, Akita Prefecture, Northeast Japan. J. Geol. Soc. Japan 107, 354–357.

Terakado, Y., 2001b. Re-Os dating of the Kuroko ores from the Wanibuchi Mine, Shimane Prefecture, southwestern Japan. Geochem. J. 35, 169–174.

Tessalina, S.G., Bourdon, B., Maslennikov, V.V., Orgeval, J.-J., Birck, J.-L., Gannoun, A., Capmas, F., Allègre, C.-J., 2008. Osmium isotope distribution within the Palaeozoic Alexandrinka seafloor hydrothermal system in the Southern Urals, Russia. Ore Geol. Rev. 33, 70–80.

Xiong, Y., Wood, S., 1999. Experimental determination of the solubility of ReO_2 and the dominant oxidation state of rhenium in hydrothermal solutions. Chem. Geol. 158, 245–256.

Yin, X.B., Zeng, Z.G., Li, S.Z., Wu, L., Wang, X.Y., Zhang, G.L., Chen, S., 2011. Determination of trace elements in sulfide samples by inductively coupled plasma-mass spectrometry. Chinese J. Anal. Chem. 39, 1228–1232 (in Chinese with English abstract).

Zierenberg, R.A., Fouquet, Y., Miller, D.J., Bahr, J.M., Baker, P.A., Bjerkgard, T., Brunner, C.A., Duckworth, R.C., Gable, R., Geiskes, J., Goodfellow, W.D., Groschel-Becker, H.M., Guerlin, G., Ishibashi, J., Iturrino, G., James, R.H., Lackschewitz, K.S., Marquez, L.L., Nehlig, P., Peter, J.M., Rigsby, C.A., Schultheiss, P., Shanks, W.C.III, Simoneit, B.R.T., Summit, M., Teagle, D.A.H., Urbat, M., Zuffa, G.G., 1998. The deep structure of a sea-floor hydrothermal deposit. Nature 392, 485–488.

771 **Figure Captions**

772

773 **Fig. 1**. Locations of seafloor massive sulfide samples from deep-sea hydrothermal
774 fields.

775

776 **Fig. 2.** Examples of Fe-Cu-Zn sulfide assemblages in seafloor massive sulfides. (a)
777 Photomicrograph of Fe-rich massive sulfide in sample 113.1GTV-1 showing euhedral
778 pyrite grains and collomorph pyrite. (b) Cu-rich massive sulfide in sample
779 MAR05-TVG1-9. (c) Zn-rich massive sulfide containing minor chalcopyrite and
780 pyrite in sample 26.1GTV1. (d) Back-scattered electron microprobe images of the
781 mineral texture in sample IR05-TVG13-4-2 shows sphalerite that has replaced barite,
782 and sphalerite containing smaller grain of pyrite. (e) Massive pyrite containing
783 Pb-sulfide microcrystallite in sample EPR05-TVG1-2-4. (f) Massive pyrite containing
784 smaller grain of galena in sample 26.2GTV-2. Observations were conducted using a
785 TESCAN VEGA 3 LMH scanning electron microscope. Ba-barite; Sp-sphalerite;
786 Py-pyrite; Cpy-chalcopyrite; Gn-galena.

787

788 **Fig. 3.** (a) Os concentrations, (b) Re concentrations, (c) $^{187}Os/^{188}Os$ values, and (d)
789 $^{187}Re/^{188}Os$ values in seafloor massive sulfides, hydrothermal precipitates,
790 hydrothermal fluids, hydrothermal plumes, metalliferous sediment, MORBs,
791 peridotites, sulfides in MORBs, and sulfides in peridotites. Seafloor massive sulfide
792 data is from Brügmann et al. (1998) and Ravizza et al. (1996) and this work.

High-temperature (HT), low-temperature (LT) hydrothermal fluid and hydrothermal plume data are from Sharma et al. (2000, 2007). TAG LT hydrothermal precipitate and metalliferous sediment data are from Ravizza et al. (1996). MORBs and sulfides in MORBs data are from Schiano et al. (1997) and Gannoun et al. (2007). Abyssal peridotite and sulfides in peridotite data are from Snow et al. (1995) and Harvey et al. (2006). Seawater data is from Peucker-Ehrenbrink and Ravizza (2000).

Fig. 4. (a) Re concentrations, (b) Os concentrations, (c) $^{187}Os/^{188}Os$ ratios, (d) $^{187}Re/^{188}Os$ ratios of different sulfide mineral assemblages from the seafloor massive sulfide samples. Red diamond symbols indicate Re concentrations, Os concentrations, $^{187}Os/^{188}Os$ ratios, and $^{187}Re/^{188}Os$ ratios of different sulfide mineral assemblages. Blue crosses indicate the average value of Re concentrations, Os concentrations, $^{187}Os/^{188}Os$ ratios, and $^{187}Re/^{188}Os$ ratios of different sulfide mineral assemblages.

Fig. 5. (a) $^{187}Re/^{188}Os$ vs. $^{187}Os/^{188}Os$ plot; (b) $^{187}Os/^{188}Os$ vs. Os concentration plot. Mixing curves between seawater and MORBs with a mixing parameter $r_{SB} = [^{188}Os]_{MORBs}/[^{188}Os]_{Seawater} = 0.1$, which fit most of the Os data of massive sulfides. Mixing curves between seawater and abyssal peridotites with a mixing parameter $r_{SP} = [^{188}Os]_{abyssal\ peridotites}/[^{188}Os]_{Seawater} = 0.1$, which fit some of the Os data of massive sulfides. Mixing curves between seawater and sulfides in MORBs and abyssal peridotites with mixing parameter $r_{SSB} = [^{188}Os]_{sulfides\ in\ MORBs}/[^{188}Os]_{Seawater} = 0.1$, and $r_{SSP} = [^{188}Os]_{sulfides\ in\ abyssal\ peridotites\ MORBs}/[^{188}Os]_{Seawater} = 0.1$, respectively. r reflects the

extent of curvature of the mixing curve (Langmuir et al., 1978). $[^{188}Os]_{Seawater}$, $[^{188}Os]_{MORBs}$, $[^{188}Os]_{abyssal\ peridotites}$, $[^{188}Os]_{sulfides\ in\ MORBs}$, and $[^{188}Os]_{sulfides\ in\ abyssal\ peridotites}$ are the concentrations of ^{188}Os in seawater, MORBs, abyssal peridotites, sulfides of MORBs, and sulfides of abyssal peridotites.

Fig. 6. Variations of (a) Pb content and Os/Re ratio, (b) Fe content and Re content, (c) Cu content and Re content, and (d) Zn content and Re content in seafloor massive sulfide samples. Re content of massive sulfide samples < 1 ppb, there is a postive correlation between Re and Fe. Re content > 10 ppb, there is a negative correlation between Re and Fe in massive sulfides.

837 **Table 1** Description of seafloor massive sulfide samples.

838

839 **Table 2** Re-Os isotopic compositions of seafloor massive sulfides.

840

Research highlights

- Seawater is a significant source of Re and Os in seafloor massive sulfides
- Initial $^{187}Os/^{188}Os$ ratios of ancient sulfides can trace ancient seawater component
- $^{187}Os/^{188}Os$ ratios of seafloor massive sulfides is not controlled by mineral facies
- Os is enriched in low-temperature conditions
- Global seafloor sulfide deposits contain roughly 4 tonnes of Re and 8 kg of Os

Figure 1

Click here to download high resolution image

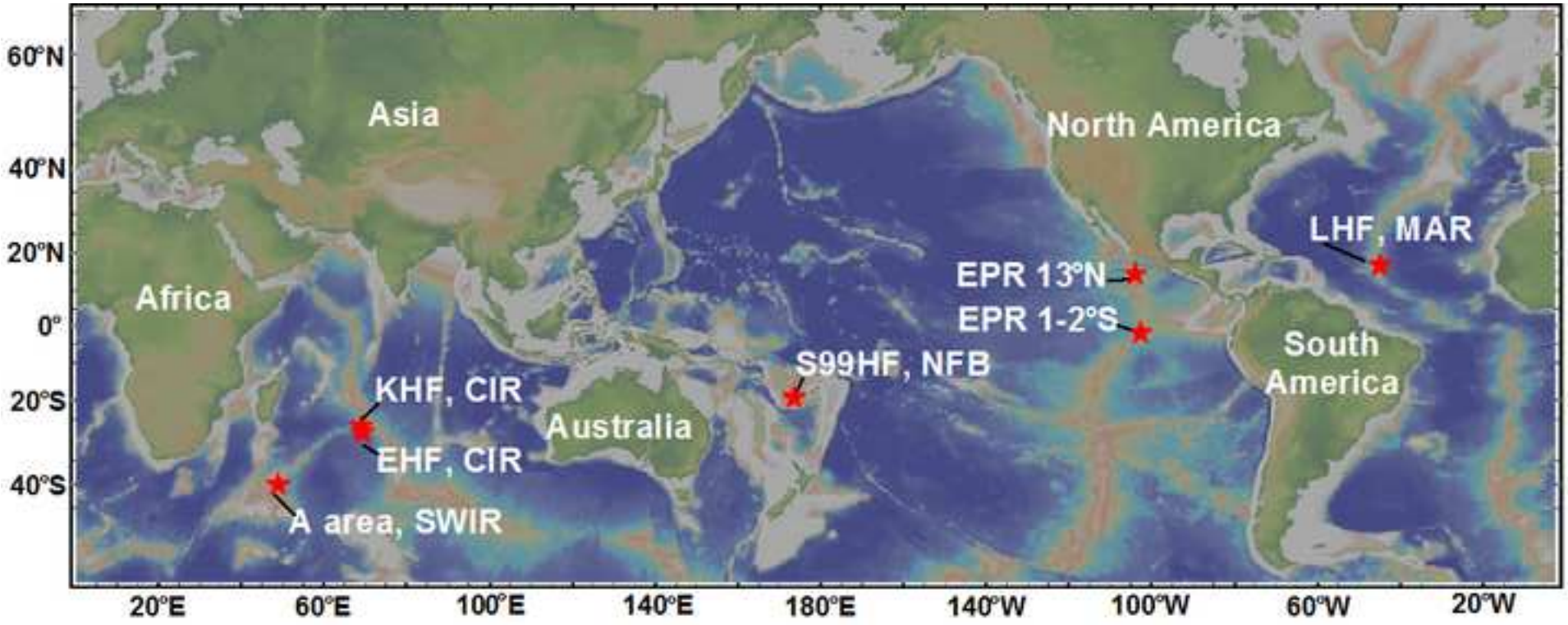

Figure 2

Click here to download high resolution image

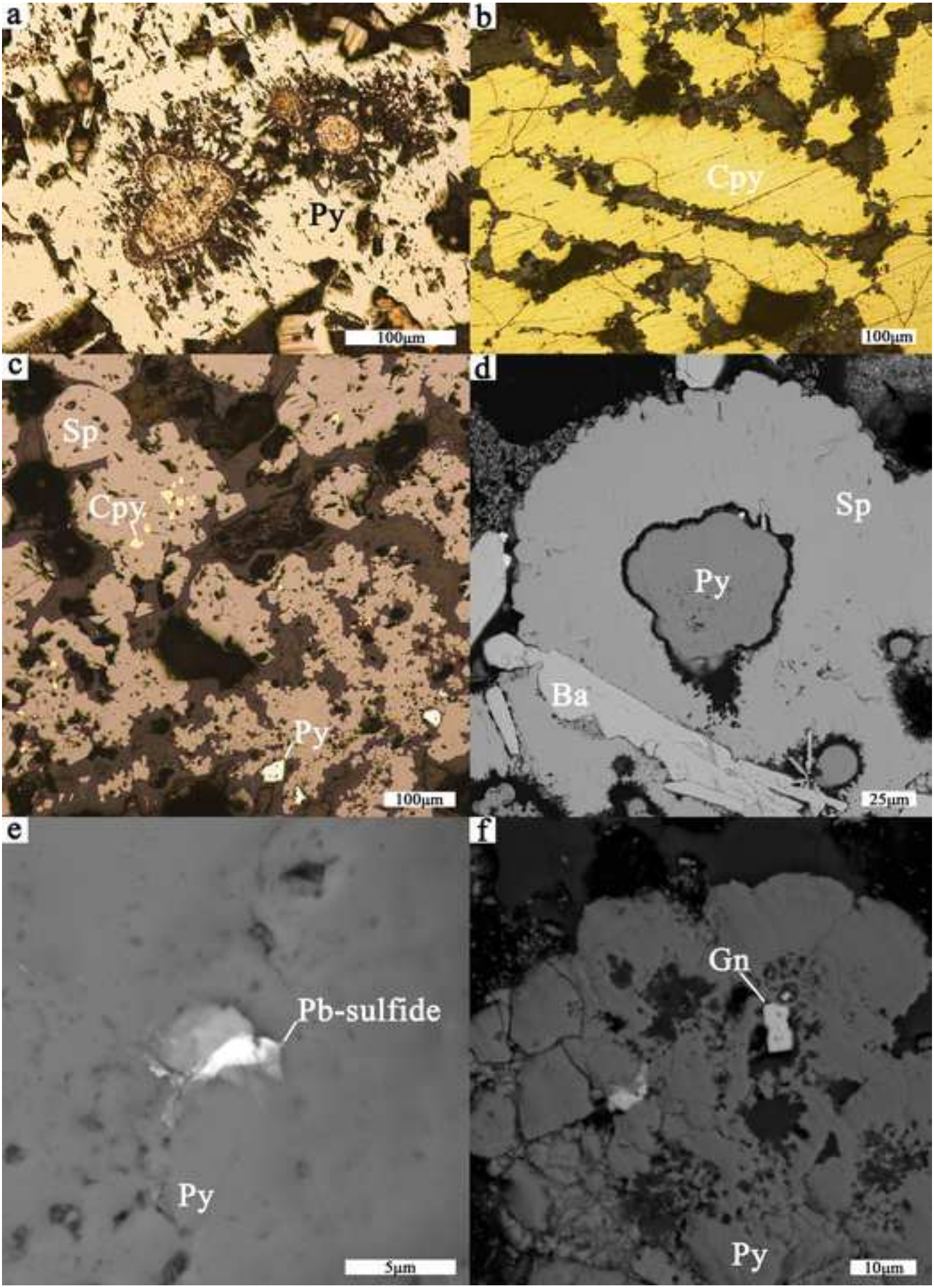

Figure 3

Click here to download high resolution image

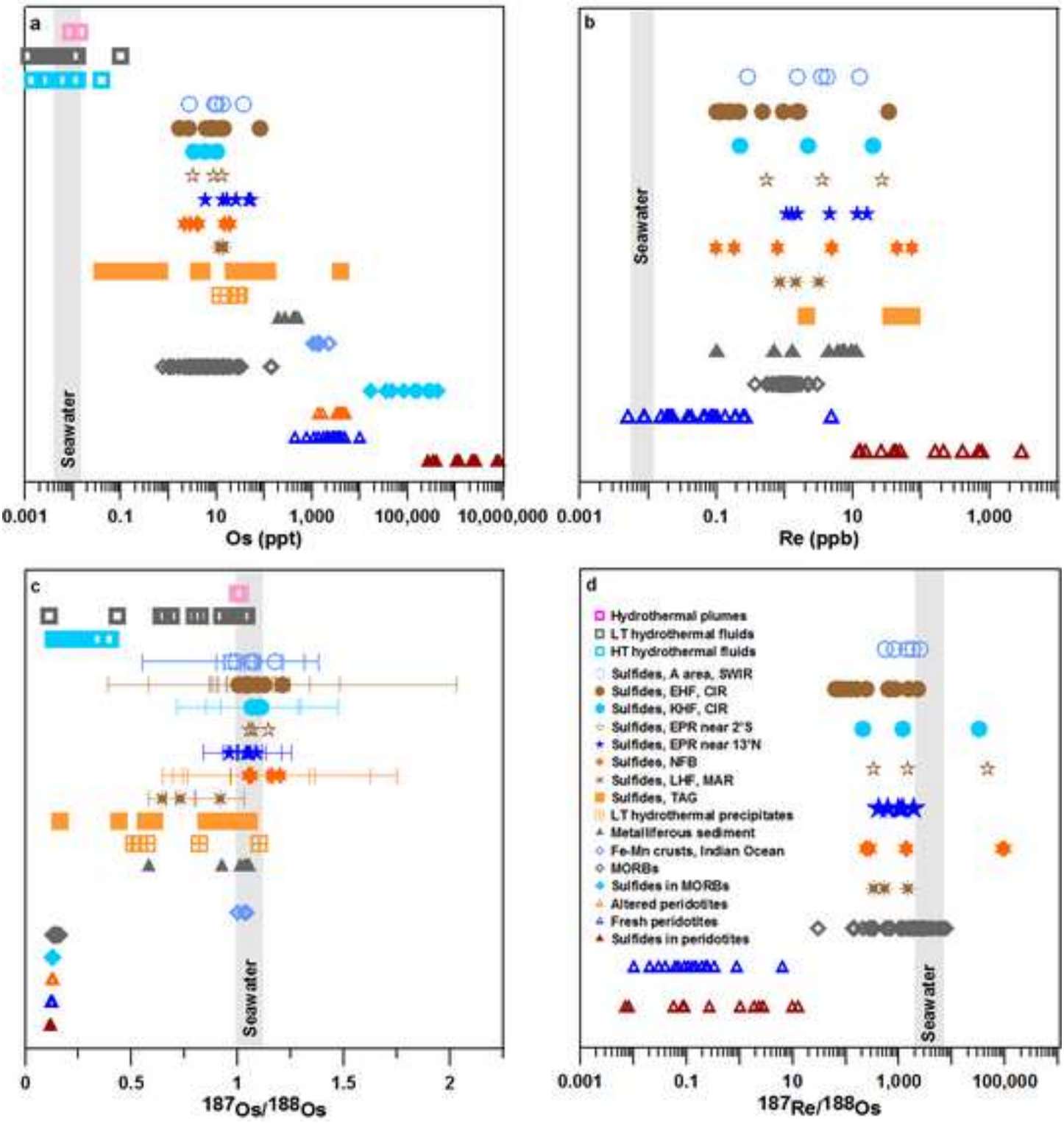

Figure 4

Click here to download high resolution image

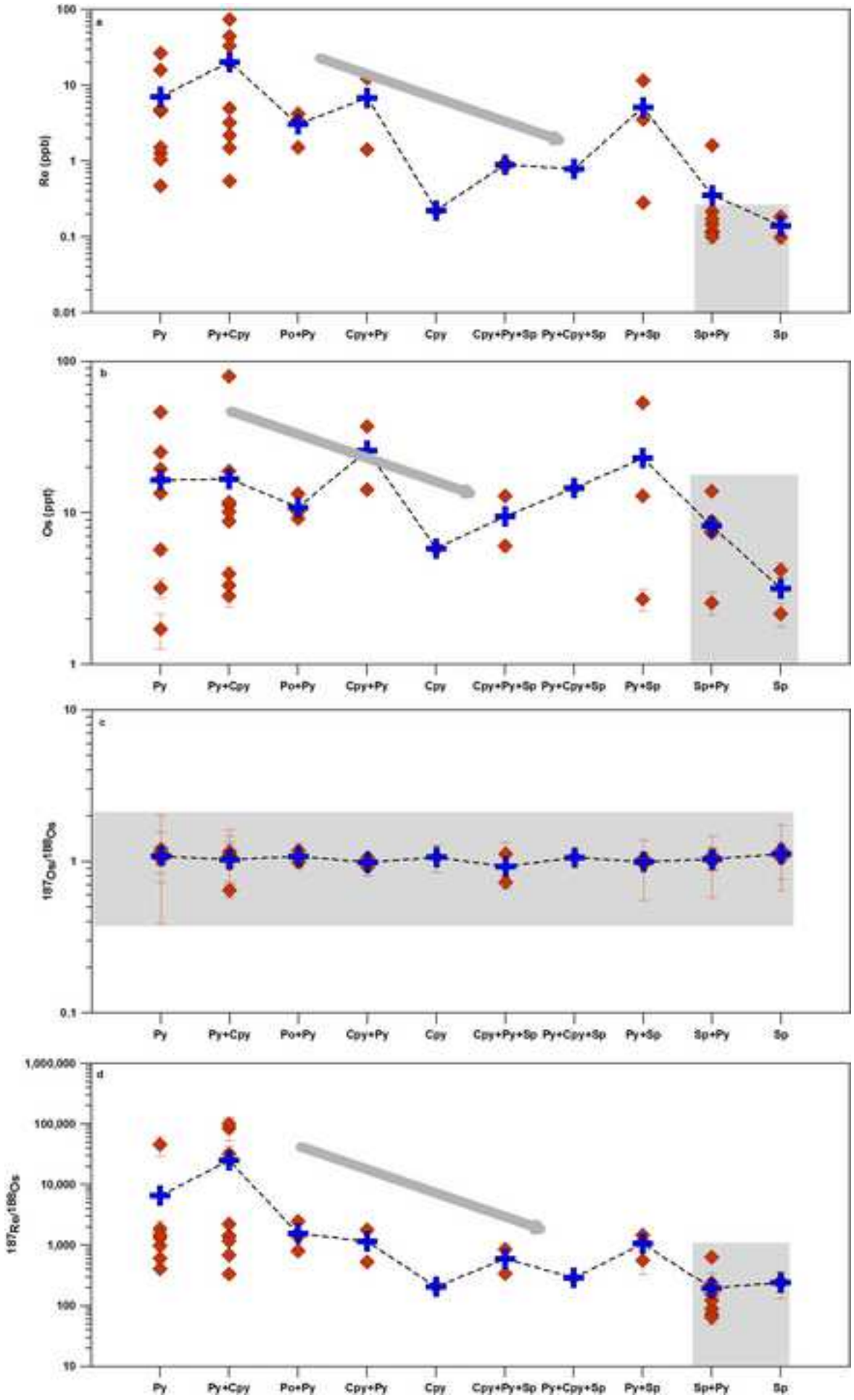

Figure 5

Click here to download high resolution image

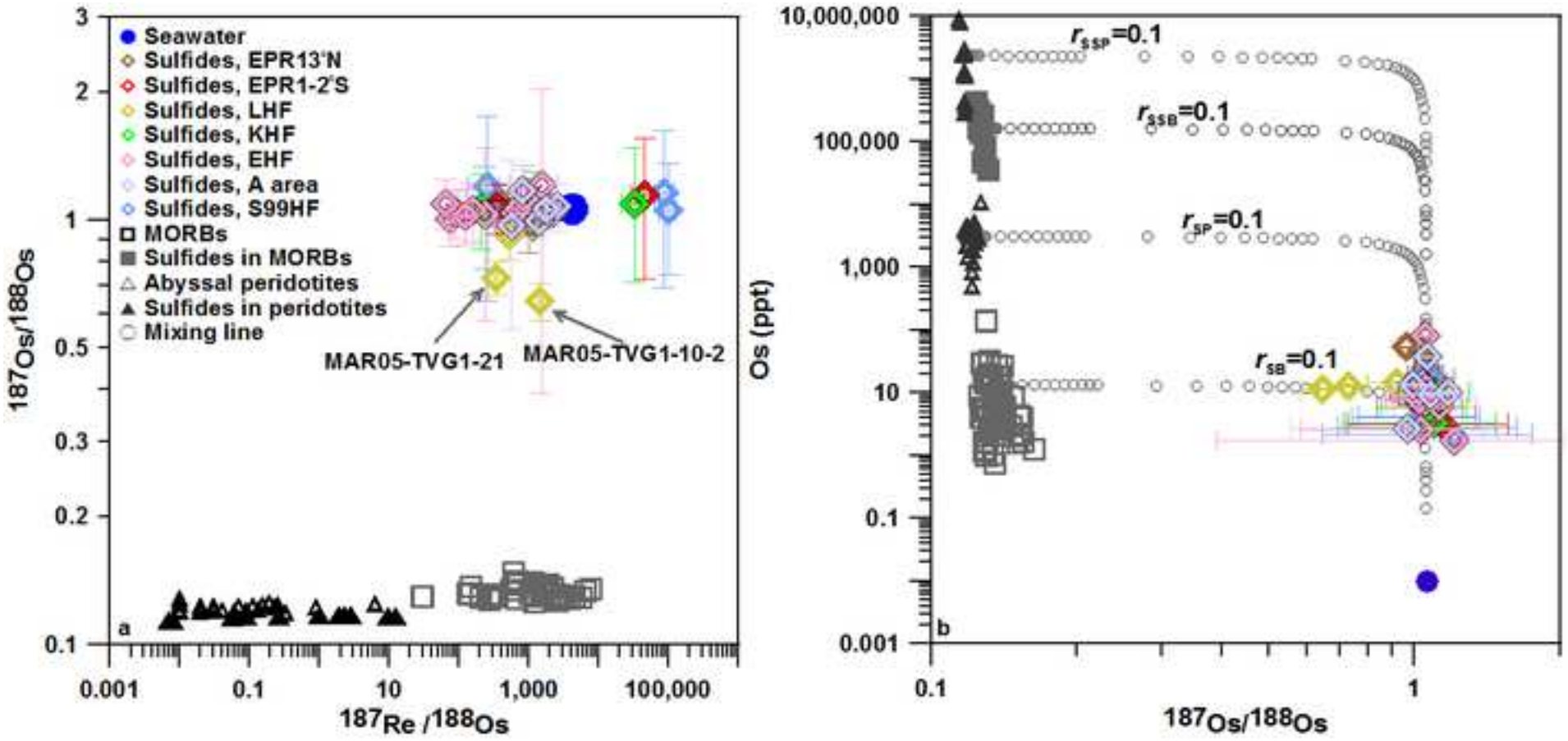

Figure 6

Click here to download high resolution image

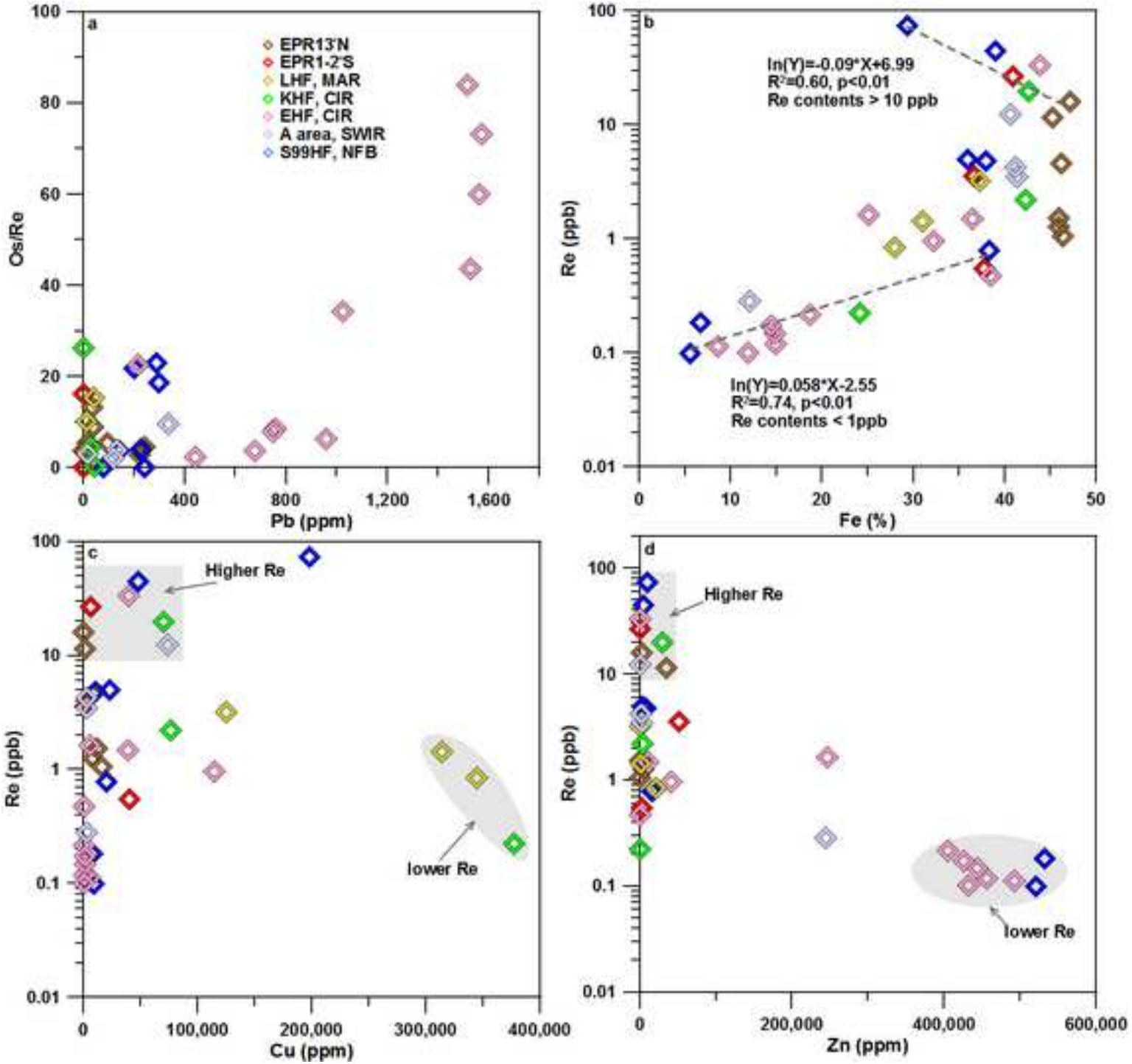

Table 1
Click here to download Table: Table 1.doc

Table 1 Description of seafloor massive sulfide samples.

Field	Sample No.	Latitude	Longitude	Water depth (m)	Description	Sulfide mineralogy
Fast-spreading mid-ocean ridge						
13°N, EPR	EPR05-TVG1-2	12°42.669´N	103°54.426´W	2,628	Fe-rich massive sulfides coated with tan Fe hydroxides, and small conduits	Py +++; Sp +, Cpy +
13°N, EPR	EPR05-TVG1-3	12°42.669´N	103°54.426´W	2,628	Fe-rich massive sulfides coated with tan Fe hydroxides, and oxidized pyrite aggregates	Py +++; Cpy +, Sp +
13°N, EPR	EPR05-TVG2-1	12°42.678´N	103°54.414´W	2,633	Fe-rich massive sulfides coated with tan Fe hydroxides and many elliptical cavities, showing development of mineral zoning	Py +++, Mc +++; Sp +
Super-fast spreading mid-ocean ridge						
1-2°S, EPR	20III-S4-TVG1-1	1°22.130´S	102°37.360´W	2,747	Porous chimney fragment coated with tan Fe hydroxides and partially filled conduits	Py+++; Mc+, Cpy+; Sp+
1-2°S, EPR	20III-S4-TVG1-2	1°22.130´S	102°37.360´W	2,747	Chimney fragment coated with tan Fe hydroxides	Py +++, Cpy ++; Mc ++; Sp+
1-2°S, EPR	20III-S6-TVG3	2°09.102´S	102°38.760´W	2,921	Outer chimney wall fragment coated with red brown Fe hydroxides and white anhydrite layer	Mc +++, Py +++; Sp ++; Cpy +
Slow-spreading mid-ocean ridge						
LHF, MAR	MAR05-TVG1-9	14°45.186´N	44°58.772´W	3,025	Porous Cu-rich massive sulfide	Cpy +++; Py ++
LHF, MAR	MAR05-TVG1-10	14°45.186´N	44°58.772´W	3,025	Fragment with gypsum, amorphous silica, disseminated marcasite and chalcopyrite	Cpy +++; Py ++
LHF, MAR	MAR05-TVG1-21	14°45.186´N	44°58.772´W	3,025	Cu-rich massive sulfides fragment with small cavities	Cpy +++; Sp +; Py+
Intermediate-spreading mid-ocean ridge						
KHF, CIR	IR05-TVG9	25°19.221´S	70°02.420´E	2,437	Chimney fragment with finely bladed chalcopyrite	Py +++; Cpy +
KHF, CIR	19III-S12-TVG6	25°09.228´S	70°04.482´E	2,443	Porous Cu-rich sulfide fragment with yellowish brown oxides in the cavities, local light green secondary Cu sulfides	Cpy +++
EHF, CIR	IR05-TVG12	23°52.678´S	69°35.808´E	3,293	Grey black Zn-rich massive sulfides coated with red to brown oxide crusts, nodular structure in the outside	Sp +++; Py ++, Mc ++
EHF, CIR	IR05-TVG13-4-1	23°52.684´S	69°35.795´E	3,292	Oxidized columnar chimney coated with red brown oxides,	Cpy +++; Mc++, Sp++,

					and fluid conduits	Py++
EHF, CIR	IR05-TVG13-9.1	23°52.684´S	69°35.795´E	3,292	Irregular crust consisted of red brown to yellowish green oxide, anhydrite and gypsum, with disseminated sulfides	Py+++
EHF, CIR	IR05-TVG13-9.2-1	23°52.684´S	69°35.795´E	3,292	Chimney fragment with red, brown and yellowish green mixture of oxide, anhydrite and gypsum	Mc+++; Cpy++, Sp++, Py++
EHF, CIR	19III-S18-TVG9	23°52.638´S	69°35.850´E	3,282	Porous Fe-Cu rich sulfides with minor sulfates	Py+++; Mc++, Sp++, Cpy++
Super-slow spreading mid-ocean ridge						
A area, SWIR	19II-S7-TVG4	37°47.004´S	49°28.176´E	2,781	Black porous massive sulfides	Sp+++, Py++; Cpy+
A area, SWIR	20V-S35-TVG17	37°46.812´°S	49°38.886´E	2,783	Massive sulfide with dark brown oxide crust	Po++, Py++; Cpy+
A area, SWIR	21VII-TVG22	37°56.316´S	49°15.894´E	1,443	Fe-rich chimney fragment coated with grey amorphous silica, conduits partially in-filled with oxides	Cpy+++, Py+++; Mc+, Sp+
Back-arc basin						
S99HF, NFB	113.1GTV	16°57.322´S	173°54.970´E	1,967	Porous massive sulfide	Py++, Cpy++
S99HF, NFB	42GTV	16°57.533´S	173°54.978´E	1,975	Cu-rich chimney fragment with conduits	Cpy+++; Py++, Mc++
S99HF, NFB	26.1GTV	16°57.602´S	173°54.991´E	1,976	Inner Zn-rich chimney wall fragment with yellowish brown oxides	Sp+++; Mc+, Cpy+
S99HF, NFB	26.2GTV	16°57.602´S	173°54.991´E	1,976	Greyish Zn-rich chimney fragment with local honeycomb structure and coarse black sphalerite crystals	Sp+++; Mc+, Cpy+

Py-pyrite; Mc-marcasite; Cpy-chalcopyrite; Sp-sphalerite; Po-pyrrhotite. +++: abundant (>30%); ++: major (5-30%); +: minor (≤5%).

Table 2
Click here to download Table: Table 2.doc

Table 2 Re-Os isotopic compositions of seafloor massive sulfides.

Sample No.	Mineralogy	Re	±2σ	Os	±2σ	$^{187}Re/^{188}Os$	±2σ	$^{187}Os/^{188}Os$	±2σ	Initial $^{187}Os/^{188}Os$	Fe	Cu	Zn	Pb
East Pacific Rise near 13°N														
EPR05-TVG1-2-1	Py	1.26	0.03	16.70	0.73	410.5	43.7	1.090	0.117	1.090	45.9	8169	4,170	35.1
EPR05-TVG1-2-5	Py	1.53	0.02	13.50	0.50	610.6	52.7	1.038	0.094	1.038	45.9	11,430	488	39.9
EPR05-TVG1-3-1	Py	4.59	0.02	25.11	0.55	987.6	46.9	1.057	0.056	1.057	46.2	8,272	6,083	94.7
EPR05-TVG1-3-2	Py	1.05	0.02	5.74	0.44	990.6	187.1	1.046	0.209	1.046	46.4	15,935	141	17.0
EPR05-TVG2-1-1	Py	15.91	0.07	46.18	0.73	1,857.6	58.9	1.037	0.039	1.036	47.1	227	2,801	223.5
EPR05-TVG2-1-6	Py+Sp	11.54	0.04	53.36	0.78	1,155.6	33.3	0.961	0.034	0.961	45.2	1610	34,790	243.0
East Pacific Rise near 1-2°S														
20III-S4-TVG1-1-1	Py	26.80	0.09	3.21	0.45	45,589.5	16,091.1	1.143	0.416	1.141	40.9	5,958	865	1.15
20III-S4-TVG1-2-1	Py+Cpy	0.55	0.02	8.85	0.48	334.0	45.0	1.070	0.145	1.070	37.8	40,054	2,334	0.80
20III-S6-TVG3	Py+Sp	3.54	0.02	12.95	0.49	1,475.2	129.8	1.054	0.098	1.054	36.6	1,393	51,142	0.70
Logatchev hydrothermal field, MAR														
MAR05-TVG1-10-2	Py+Cpy	3.20	0.02	11.35	0.45	1,450.3	133.4	0.645	0.066	0.645	37.3	125,219	267	13.3
MAR05-TVG1-9	Cpy+Py	1.42	0.03	14.31	0.69	528.7	60.7	0.917	0.114	0.917	31.0	314,180	1,422	14.7
MAR05-TVG1-21	Cpy+Py+Sp	0.84	0.02	12.92	0.47	339.5	29.2	0.730	0.066	0.730	27.9	344,227	20,820	41.4
Kairei hydrothermal field, CIR														
IR05-TVG9-1	Py+Cpy	2.21	0.03	10.22	0.69	1,174.5	193.1	1.109	0.189	1.109	42.3	76,665	3,054	27.9
IR05-TVG9-3	Py+Cpy	19.78	0.07	3.31	0.45	32,379.8	10,888.0	1.093	0.380	1.092	42.7	70,004	30,130	45.9
19III-S12-TVG6	Cpy	0.22	0.02	5.84	0.46	206.3	44.4	1.067	0.215	1.067	24.1	376,988	801	1.54
Edmond hydrothermal field, CIR														
IR05-TVG12-5-4	Sp+Py	0.11	0.02	2.56	0.43	237.7	108.3	1.029	0.450	1.029	8.61	5,560	492,389	216
IR05-TVG12-8-2	Sp+Py	1.63	0.02	13.96	0.49	629.8	52.0	1.041	0.090	1.041	25.1	5,287	246,400	758

IR05-TVG12-8-3	Sp+Py	0.22	0.02	7.40	0.46	157.9	28.1	1.052	0.167	1.052	18.6	854	405,000	1,024
IR05-TVG12-9-1	Sp+Py	0.12	0.02	8.68	0.47	73.4	15.9	1.004	0.138	1.004	14.9	912	455,500	1,571
IR05-TVG12-11	Sp+Py	0.15	0.02	8.84	0.46	90.0	16.6	1.038	0.137	1.038	14.9	1,010	443,500	1,560
IR05-TVG12-12	Sp+Py	0.17	0.02	7.58	0.45	123.3	22.4	1.025	0.153	1.025	14.4	1,058	425,900	1,528
IR05-TVG12-14	Sp+Py	0.1	0.0	8.4	0.5	64.7	15.2	1.094	0.149	1.094	11.9	938	432,404	1,515
IR05-TVG13-4-1	Cpy+Py+Sp	1.0	0.0	6.0	0.5	861.2	159.5	1.125	0.215	1.125	32.2	114,193	40,755	959
IR05-TVG13-9.1	Py	0.5	0.0	1.7	0.4	1,514.3	1,002.3	1.209	0.820	1.209	38.4	803	270	677
IR05-TVG13-9.2-1	Py+Cpy	1.5	0.0	11.8	0.5	684.0	65.1	1.058	0.105	1.058	36.4	39,067	10,404	748
19III-S18-TVG9	Py+Cpy	33.5	0.1	79.9	1.1	2,264.0	56.2	1.048	0.034	1.048	43.8	39,713	332	442
A area, SWIR														
19II-S7-TVG4	Py+Sp	0.3	0.0	2.7	0.4	560.6	233.2	0.968	0.413	0.968	12.0	2,575	244,281	337
20V-S35-TVG17-3-2	Po+Py	3.5	0.0	13.3	0.5	1,399.0	120.1	0.993	0.090	0.993	41.3	2,637	2,480	134
20V-S35-TVG17-4-2	Po+Py	4.2	0.0	9.2	0.5	2,494.5	307.6	1.076	0.140	1.076	41.1	2,580	1,386	121
20V-S35-TVG17-7	Po+Py	1.5	0.0	10.2	0.5	813.9	93.1	1.174	0.140	1.174	n.a.	n.a.	n.a.	n.a.
21VII-TVG22	Cpy+Py	12.4	0.0	37.3	0.7	1,792.4	64.7	1.061	0.045	1.061	40.6	73,348	515	17.4
Sonne 99 hydrothermal field, North Fiji Basin, BAB														
113.1GTV-1	Py	4.79	0.03	19.46	0.61	1,330.4	93.8	1.053	0.087	1.053	37.9	10,357	7,875	227
113.1GTV-2	Py+Cpy	4.97	0.03	18.84	0.60	1,426.3	102.8	1.057	0.089	1.057	36.0	22,903	3,734	143
42GTV-1	Py+Cpy	44.45	0.15	2.83	0.44	85,800.7	33,324.5	1.160	0.466	1.157	39.0	48,071	5,146	240
42GTV-3	Py+Cpy	73.60	0.25	3.96	0.45	100,334.7	28,260.7	1.052	0.310	1.049	29.3	197,581	10,239	78.4
113.2GTV	Py+Cpy+Sp	0.79	0.02	14.61	0.54	291.1	25.8	1.066	0.102	1.066	38.3	20,238	15,960	297
26.1GTV-1	Sp	0.10	0.02	2.15	0.38	252.1	120.7	1.197	0.551	1.197	5.51	8,896	520,500	200
26.2GTV-1	Sp	0.18	0.02	4.21	0.45	234.0	66.1	1.051	0.287	1.051	6.64	7,882	531,900	289

Py-Fe sulfide, including pyrite and marcasite; Cpy-chalcopyrite; Sp-Zn sulfide, including sphalerite and wurtzite; Po-pyrrhotite. Unit ppb for Re; ppt for Os; % for Fe; ppm for Cu, Zn and Pb; n.a. not analyzed. Initial $^{187}Os/^{188}Os$ composition has been calculated at 2 ka.